Earthquake scenario selection of Tindharia landslide in India

Neharika, G.N.S
Research Assistant, International Institute of Information Technology, Geotechnical Research Laboratory, Gachibowli, Hyderabad-500008, Telangana, India
Neelima Satyam, D.
Associate Professor, Indian Institute of Technology, Discipline of Civil Engineering, Simrol, Indore-453552, Madhya Pradesh, India

Received July 2021, Accepted August 2021

Abstract

Earthquake-induced landslides can affect people and structures as a result of significant ground shaking or regardless of the intensity. A suitable design ground motion helps to mitigate the impact of such landslides. The most commonly used design ground motion in slope stability analysis is based on probabilistic seismic hazard maps. Uncertainties in the selection of expected ground motion levels have been ignored. The present study is conducted based on improvised fully probabilistic approach, which provides the total probability of slope failure in a particular period under seismic loading by addressing all possible scenarios. This approach is applied to the seismically active Tindharia slope located in Darjeeling, India. The total probability of seismic slope failure obtained in the next 50 years is 30% and the most probable peak-ground acceleration that triggers a landslide is 0.12g. Design peak-ground acceleration predicted from the next 475-year probabilistic seismic hazard map is 1.02g. In the present study, the significant difference in the design peak-ground acceleration from probabilistic seismic-hazard analysis and fully probabilistic approach is observed. The study suggests that the seismic landslide hazard may be overestimated or underestimated when used in the design of ground intensity obtained by conducting PSHA.

1. Introduction:

Earthquake-induced landslides pose major threats worldwide, especially in mountainous zones (Liao and Lee, 2000). India has experienced several destructive earthquakes ($M_w \geq 8.0$) that have caused deadly landslides, which have had an impact on the human environment in many ways. In this country, 70% of highly vulnerable landslides have been observed in the Himalayan region, Northeast India, Eastern Ghats, and Western Ghats.

Several methods and evaluation studies are proposed to determine the landslide hazard and conduct a susceptibility assessment (Guzzetti et al., 1999). The methods are either quantitative or qualitative approaches based on knowledge, experience, numerical expressions, methods, and computer-based models. Seismically induced landslide analysis considers not only the well-measured material properties but also proper ground-motion selection.

Many researchers have developed seismically induced hazard maps in terms of susceptibility or probability on a regional or global scale. Most of the hazard maps are developed by estimating slope parameters using a global information system that provides the rough hazard level of the specific site. The statistical and deterministic

approaches focus on landslide susceptibility that helps determine where landslides are likely to occur through the use of physically based models regardless of triggering conditions (Van Westen et al. 2008; Lee et al., 2008). In current engineering practice, the quantified risk levels of the regional or global scale have been identified using hazard maps produced by probabilistic approach (Raghukanth and Iyenger, 2007). The triggering peak ground acceleration (PGA) in the slope stability analysis has been computed from probabilistic hazard maps. Most commonly, the PGA that initiates failure of the slope is measured from 475 years of 10% probability seismic hazard maps (Wang et al., 2017). The hazard maps developed based on an earthquake catalogue (EC) are not restricted to the use of regional ground-motion prediction equation (GMPE) only. The pseudo probabilistic, statistical, and deterministic approach provides a conservative estimation of seismic landslide hazards. Most of the studies observed uncertainty regarding the earthquake scenario.

The improvised fully probabilistic approach (Alexey et al., 2020) has been applied in the present study to estimate the consistent earthquake scenario for seismic slope stability. The method handles the uncertainties in the data and provides reasonable hazard management. The framework of the approach aims to find the total probability of the slope failure under various ground-shaking levels (Del Gaudio et al., 2003). Some researchers have used this approach to develop the annual frequency of exceedance for the given sliding displacements (Rathje etal., 2008; Martino et al., 2019; Del Gaudio et al., 2003).

The present study aims to examine the impact of the Tindharia landslide, which occurred because of the September 18, 2011 earthquake and destroyed the World Heritage Site in the area. The landslide occurred in seismic zone IV in the Darjeeling region in West Bengal, India. This zone is highly vulnerable to earthquakes and is seismically active due to many seismic sources. Thus, considering the suitable selection of the earthquake scenario is important for the seismically induced landslide hazard assessment.

2. Methodology:

Fully probabilistic approach

A fully probabilistic approach represents the entire probability chain of the seismically induced landslide from strong motion prediction to mode of deformation. The approach accounts for two essential stages of calculation: evaluation of probability of occurrence of various PGA (y_i) within a certain period and determination of conditional probability at which the landslide triggers a given PGA. The total probability of the slope in the next T years is calculated using the following equation:

$$P_T(\text{slope failure}) = \sum_j \sum_i w_j P_T(\text{PGA} = y_i).\, P(\text{slope failure} \mid y_i, \text{model j}) = \sum_j \sum_i w_j p_{ij}, \quad (1)$$

where P_T (PGA = y_i) occurrence probability of PGA (y_i) in a certain time interval and P(SF| y_i, model j) is the probability of the slope failure under seismic loading (y_i) for

slope model j. Geo-mechanical models of slope were ranked by weight w_j, where $\sum_j w_j = 1$.

Probability of occurrence of PGA

PSHA is involved in the development of seismic hazard curves to address engineering safety issues in specific hazard levels (Raghukanth and Iyengar, 2007). The main goal of the analysis is to determine the probability of exceedance of a particular PGA in specified time intervals of seismic hazard curves (Cornell, 1968). The analysis is based on all possible sources in the site with all possible earthquake magnitudes, site-to-source distance, and GMPE. The calculation of all the sources that exceed the acceleration a is

$$\lambda(\mathrm{PGA} > y) = \sum_{i=1}^{n_{sources}} v(\mathrm{M_i} > m_{min}) \sum_{j=1}^{n_M} \sum_{j=1}^{n_R} \mathrm{P}\left(\mathrm{PGA} > \mathrm{y_i} \mid \mathrm{m_j}, \mathrm{r_j}\right). \mathrm{P}(\mathrm{M_i} = \mathrm{m_k}) . \mathrm{P}(\mathrm{R_i} = \mathrm{r_k}), \quad (2)$$

Where, $n_{sources}$ represent the potential earthquake sources, and n_M and n_R represent the number of possible earthquakes and distances. $P(M_i = m_k)$ and $P(R_i = r_k)$ are the probability of magnitudes and distances in source i. *v*, the average rate of the threshold magnitude greater than the minimum magnitude, can be expressed as

$$v = 10^{a-bm_o} \quad (3)$$

Where a and b parameters are constants and m_o is constant mean annual rate of exceedance. These three parameters are obtained from the EC using Gutenberg–Richter distribution.
The probability of magnitude is

$$F_M(m) = \frac{1-10^{-b(m-m_0)}}{1-10^{-b(m_{max}-m_0)}}, \quad (4)$$

Where $F_M(m)$ is the cumulative distribution function and m_{max} is the maximum magnitude that the source produces.

The $(PGA>y_i \mid m_j, r_k)$ is the probability of exceedance of the PGA for acceleration y_i for m_j and r_k. The probability of exceedance of any PGA value is derived as follows:

$$\mathrm{P}(\mathrm{PGA} > y \mid \mathrm{m}, \mathrm{r}) = 1 - \phi\left(\frac{\ln(y) - \ln(\mathrm{PGA})}{\sigma_{\ln \mathrm{PGA}}}\right) \quad (5)$$

Where, σ_{lnPGA} is the standard deviation.

The probability of exceeding the PGA value (y_i) in the next T years is

$$\mathrm{P_T}(\mathrm{PGA} > y) = 1 - \mathrm{e}^{-\lambda(\mathrm{PGA}>y).\mathrm{T}} \quad (6)$$

The probability of occurrence of a discrete set of ground motions is as follows:

$$P_T(PGA = y_i) = P_T(PGA > y_i) - P_T(PGA > y_{i+1}) \quad (7)$$

Equation (7) is used to evaluate the total probability of slope failure in equation 1.

Conditional probability of Tindharia landslide

The second step in calculating the fully probabilistic analysis is to know the probability of slope failure under seismic loading. The analysis is evaluated using Jibson probabilistic model (Jibson et al., 2000), which corresponds to Weibull distribution shown in the equation 8 The model calibrated with predicted sliding displacement (D_N) in cm, critical acceleration (a_c) and peak ground acceleration (y) based on Newmark approach (Newmark, 1965). The Newmarks approach assess the probability of slope triggering given the critical slope acceleration (a_c) and PGA value (y).

$$P(slope failure|D_N) = 0.335[1 - \exp(-0.048{D_N}^{1.565}) \quad (8)$$

Where,

$$logD_N(y) = 0.215 + [\left(1 - \frac{a_c}{y}\right)^{2.341} \left(\frac{a_c}{y}\right)^{-1.438}] \pm 0.51 \quad (9)$$

Many empirical relations are combined with Newmark's displacement (D_N) and intensity. However, in the present study, the predicted Newmark's displacement of the slope is evaluated with PGA using the above equation 9 (Romeo, 2000).

The critical acceleration (a_c) is a function of slope geometry and static factor of safety (F_s) and given as

$$a_c = (F_s - 1)gsin\alpha \quad (10)$$

Where, F_s and g are the static factor of safety and factor of gravity, and α is the dip angle of the sliding surface.

The static factor of safety is calculated using simplified limit equilibrium model of an infinite slope under certain assumptions based on Newmark approach (1965). As per the Newmarks approach, when some internal deformation accumulates the sliding mass the failure of landslide starts. When the seismic acceleration exceeds the critical value the accumulation of inner deformations takes place.

The approach considers the landslide mass sliding along planar surface. The assumptions in the model considered are as follows: the slope is homogeneous, the effect of pore pressure is negligible, the static safety factor is stress independent (constant), the sliding mass of the slope is rigid solid, and coefficients of static and dynamic friction are equal and constant. The static factor of safety (F_s) according to limit equilibrium theory is given as follows (Jibson et al., 2000):

$$F_s = \frac{c'}{yzsin\alpha} + \frac{tan\varphi}{tan\alpha} + \frac{my_w tan\varphi}{ytan\alpha} \quad (11)$$

where c' is cohesion, φ is friction angle, z is slope normal thickness, γ and γ_w are unit weight of material and ground water, α is dip angle of the sliding surface, and m is the saturated sliding mass thickness.

The soils in the area are saturated most of the year, so pore pressures are neglected from the equation 11 and paid great attention on third term of the equation.

In the next T years, the total probability of seismically induced landslide is obtained by substituting equations (8) and (7) in equation (1).

3. Details of study area:

The Tindharia slide is located at latitude and longitude of 26°51^{1}14.55^{11}N–88°20^{1}13.12^{11}E in Darjeeling hills, West Bengal, India. The landslide is beneath the century-old Darjeeling toy train used in tourism. The slope failed on September 18, 2011 after the earthquake in Sikkim, Nepal (Figure 1).

(a) (b)

Picture 1 Aerial photographs of study area: (a) front view and (b) side view (Source: Save the Hills)

The triangular debris slide was trigged initially by the earthquake, and the debris is widely spread over the entire site and deposited at the lower part of the slope. The upper part of the slope consists of colluviums and residual soils with varying thickness of 0–8m after the earthquake. After the initial earthquake-induced slope failure, the destabilization and series of failures were observed in the study area because of heavy rainfall on

September 28th, 2011. The debris had been eroded and washed away due to surface runoff. Highly weathered sandstone was exposed in some areas on the slope, revealing open cracks, especially at the top of the slope. Furthermore, destabilization and failure at the toe of the slope was observed due to stream erosion. A stream of water flowed toward the bottom of the slide and played a vital role in mass wasting and initiating further instability on the slope.

Material properties

The Tindharia landslide altered at elevation ranges of 600–800m with 30°–45°slope. According to the geological profile, the top layer of the study area is covered with residual soils and colluviums mainly with coaly shale and sandstone from the Gondwana group. A coal band is observed at the toe of the slope. The bottom layer of the slope is covered with highly weathered sandstone. The slope parameters for the hazard assessment were selected from the geological report of the study area by Kundu (2019).The soil parameter cohesion (c') and friction angle (φ) are 7.8 Kpa and 38°.The unit weight of material (γ) and groundwater (γ_w) is 19 and 9.8kN/m3. The slope normal thickness (z) and dip angle (α) are 4m and 28°. The saturated sliding mass thickness (m) is considered as 1 in the present study.

4. Preparation of EC and seismo-tectonic map:

EC preparation is the most fundamental step in PSHA. To prepare the EC, the following procedure is conducted: collection of earthquake data, homogenization of earthquake magnitude, de-clustering of the catalogue, and checking for data completeness.
The present study area is in the Bengal basin, which was seismically stable before 1930 and vulnerable after several seismic sources around the site produced remarkable ground motions. At a radius of approximately 300km from the site, magnitudes in the range of 4.0–8.0 were collected from 1932 to 2019 (91 years) and used in the present analysis. The region included active thrusts, faults, and lineaments. A total of 1,227 point sources along with 21 potential linear sources before declustering are collected along with magnitude scales, focal depth, time, and date. The point sources are collected from historical and instrumental records (USGS, ISC, and IRIS) and published literature. The linear sources are collected from the Seismotectonic Atlas of India (SEISAT 2000). The collected earthquake data are in different magnitude scales, so the homogenization of the collected data to one moment magnitude scale was conducted based on the empirical relations presented by Scordilis (2006) and Deniz and Yucemen (2010).

The de-clustering is necessary because the earthquake events collected from various sources are the raw data with good possibility of dependent events such as foreshocks and aftershocks. Furthermore, as we collected the data from various sources, the same events that were repeated with the same magnitude or with slightly different magnitudes were observed carefully and removed. The aftershocks and foreshocks from the homogenization catalogue were de-clustered based on the window method of Gardner and Knopoff (1974) using ZMAP software (Wiemer, 2001). After the removal of all

independent events, out of 1277 events a total of 189 main shock events (84.64% of total records) were in the final catalogue. The before and after de-clustering of the events for the present study are shown in the Figure 2 (a & b).

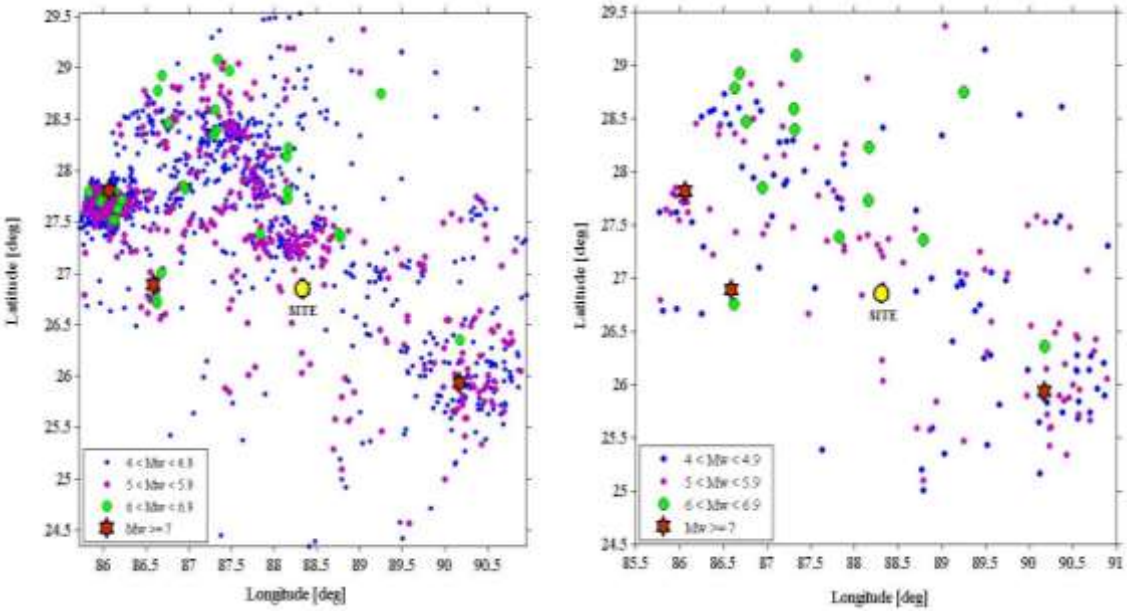

Picture 2 (a) Before and (b) after de-clustering of catalogue.

The complete catalogue with moment magnitudes of Mw>4 is summarized in Table 1. The seismo-tectonic map for the present study area is shown in Figure 3.

Table 1
Summary of final earthquake catalogue

SI No.	Moment magnitude (Mw)	Number of events
1	$4 \leq M_w < 4.5$	17
2	$4.5 \leq M_w < 5$	60
3	$5 \leq M_w < 5.5$	60
4	$5.5 \leq M_w < 6$	33
5	$6 \leq M_w < 6.5$	10
6	$6.5 \leq M_w < 7$	5
7	$M_w \geq 7$	3

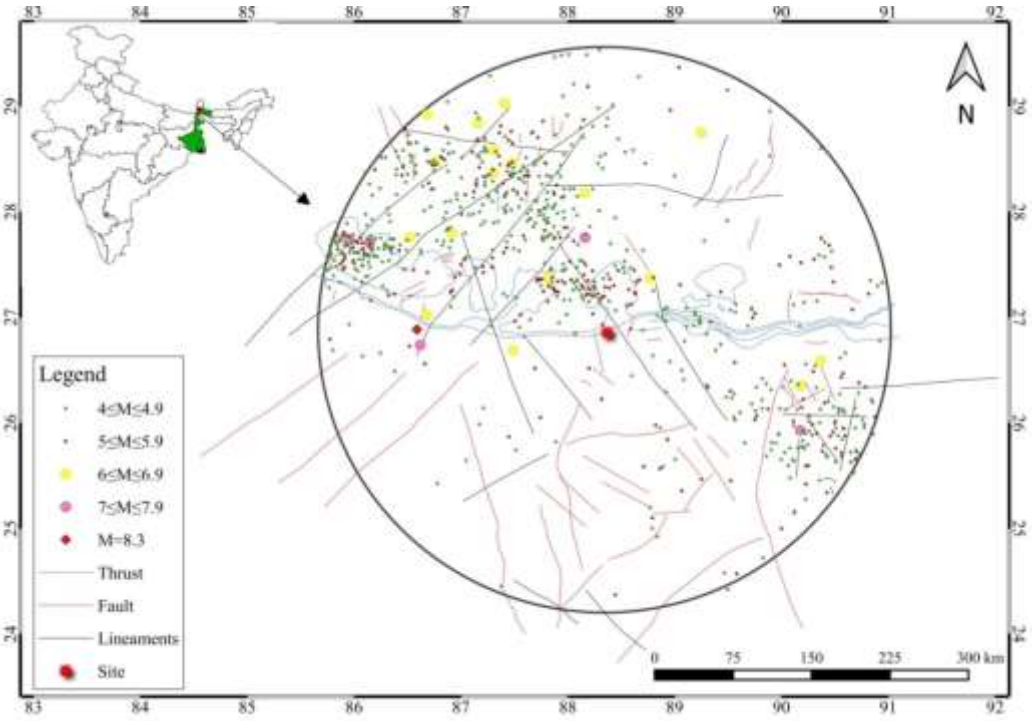

Picture 3 Location of site along with seismic tectonic features and distribution of past earthquakes (1932 to 2019) with in 300 km radius.

5. Analysis of Results and Discussion:

Data checking for completeness in terms of quality and quantity to ensure reliable results was conducted using a statistical test proposed by Stepp (1973) as shown in Figure 4.

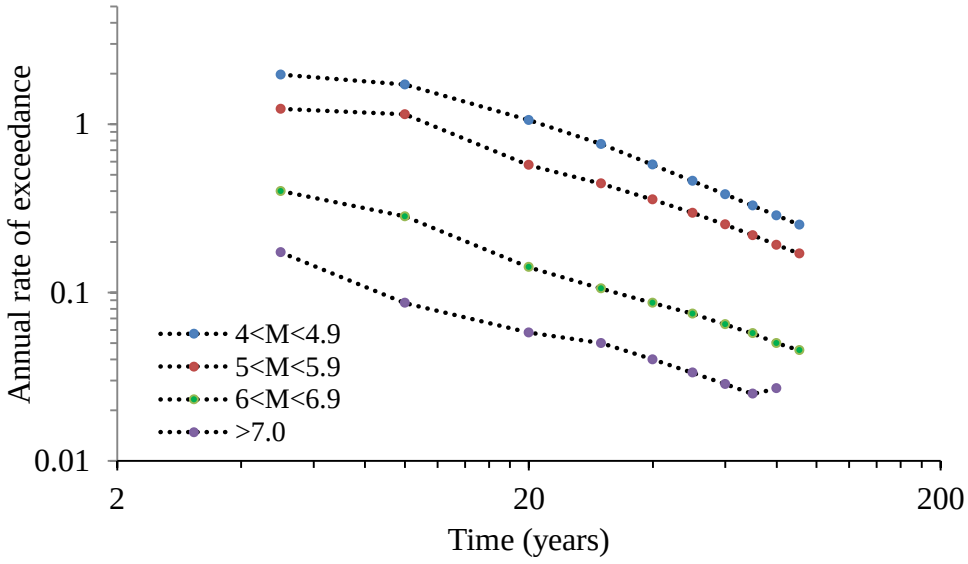

Picture 4 Data completeness based on Stepp's method.

The seismicity parameters were evaluated using Gutenberg and Richter (G–R) model (1944) for the improved EC. The distribution of the earthquake frequency in a region with respect to magnitude is only frequency magnitude distribution estimated using the G–Rrecurrence model expressed as

$$\log \lambda_m = a - b\mathrm{M_w}, \tag{12}$$

where λ_m indicates the cumulative number of earthquakes with magnitudes greater than or equal to $\mathrm{M_w}$. The 'a' parameter describes the background seismicity, i.e., mean yearly number of earthquakes in a region, and 'b' describes the relative ratio of larger shocks to smaller shocks.

From the seismic parameters, the level of seismicity of the region can be evaluated. Thus, the G–R regional recurrence relationship for the study area is presented in Figure 5. The magnitude of completeness (Mc) is minimum magnitude event, where 100% is detected (Rydelek and Sacks, 1989) as estimated by Wiemer and Wyss (2000) method using the ZMAP tool (Wiemer, 2001). The site is divided into (0.1° * 0.1°) grid size and Mc is evaluated at the center of each grid within 300km radius.

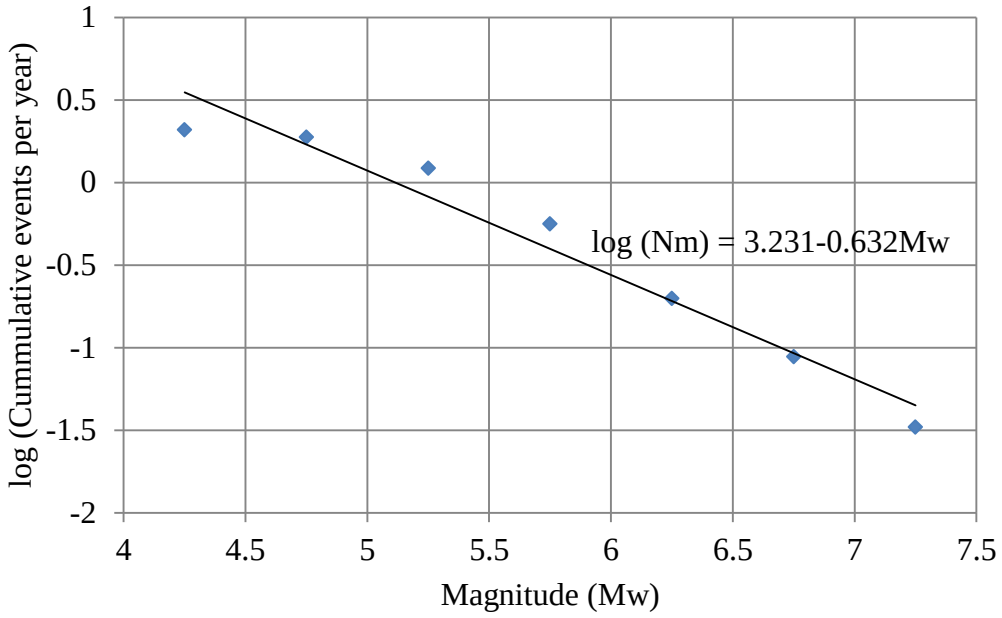

Picture 5 Frequency magnitude distribution relation of entire study area.

In the present study, the seismic parameters 'a' and 'b' are estimated to be 3.228 and 0.631. The seismic parameters obtained are comparable with those from previous studies conducted in the same region.

GMPE

The 189 seismic point sources within 300km radius from the site are distributed by one or the other nearest dynamic potential active tectonic features such as thrust, faults, and

lineaments. Thus, in the present study, the 20 line-source combinations of active faults, lineaments, and thrusts were selected for seismic hazard assessment of the study region (Table 1). The different hypocentral depth is considered within the range of 1–70 km depending on the faults for real hazard estimation.

Table 2
Details of seismic sources

SI.No	Fault Name	Shortest distance from site (km) (Rmin)	Mmax
1	East Patna Fault	190.478	7.1
2	Munger Sahastra Ridge Fault	130.129	7.2
3	Munger Sahastra Ridge	156.888	7
4	Rajmahal Fault	197.761	6.7
5	Malda Kishanganj Fault	79.037	5.3
6	Jangipur Fault	244.137	7.2
7	Gaibandha Fault	199.347	7.2
8	Debagram Bogra Fault	256.412	4.4
9	Dhubri Fault	171.615	7.8
10	Katihar Nailphamuri Fault	105.396	7
11	West Patna Fault	243.126	7.2
12	Sainthia Bahman Fault	229.488	6.4
13	GouriShankar Lineament	229.487	7
14	Everest Lineament	183.12	6.6
15	Arun Lineament	136.49	7.2
16	Kanchenjunga Lineament	89.844	5.5
17	Purnea Everest Lineament	99.734	5.7
18	Tista Lineament	10.981	7.1
19	Main Boundary Thrust	4.321	7.3
20	Main Central Thrust	8.214	8

Many researchers have developed different GMPEs for various regions of India depending on the observed and available datasets to estimate PGA. The GMPE selection among several available GMPEs is an important step because it greatly influences the final hazard assessment. The present study area consists of two zones: Bengal basin zone and northeastern Himalayan zone. The range of shear wave velocity is ranging from 100 to 3800 m/sec for Bengal Basin (Mitra et al. 2008 and Nath et al., 2010). The tectonic features of the study area are mostly influenced by those of the most active Himalayan region. Few GMPEs have been developed for the study area, but the best suited GMPE was checked and selected for the present study area is of Anbazhagan et al. (2019) which is performed with magnitude range Mw 4-9, hypo central distance range 10-750kms and shear wave velocity V_{s30} of 2000m/sec; and is expressed as follows:

$$\ln(Y) = a_1 + a_2(M-6) + a_3(9-M)^2 + a_4 \ln R + a_m \ln R(M-6) + a_7 R + \sigma \quad (12)$$

$a_m = a_5$, $(M_w < 6.0 \; and \; R < 300)$ or else is equal to a_6,

Where Y is the ground motion; a1, a2, a3, a4, am, a6, and a7 are the regression coefficients; M is the moment magnitude; R is the hypocentral distance; and σ is the standard deviation.

6. Results and discussion:

The PSHA study is performed for the evaluation of seismic hazard curves, which represent the PGA against the mean annual rate of exceedance. The seismic hazard curve shown in Figure 6 is computed using CRISIS (2007) software. The design PGA from the seismic hazard curve corresponding to 10% probability of exceedance (475-year return period) for the study area obtained is 1.02g. The PGA obtained from the seismic hazard curve is compared with the previous research result in the study area. The obtained PGA shows a good match with that provided by previous studies.

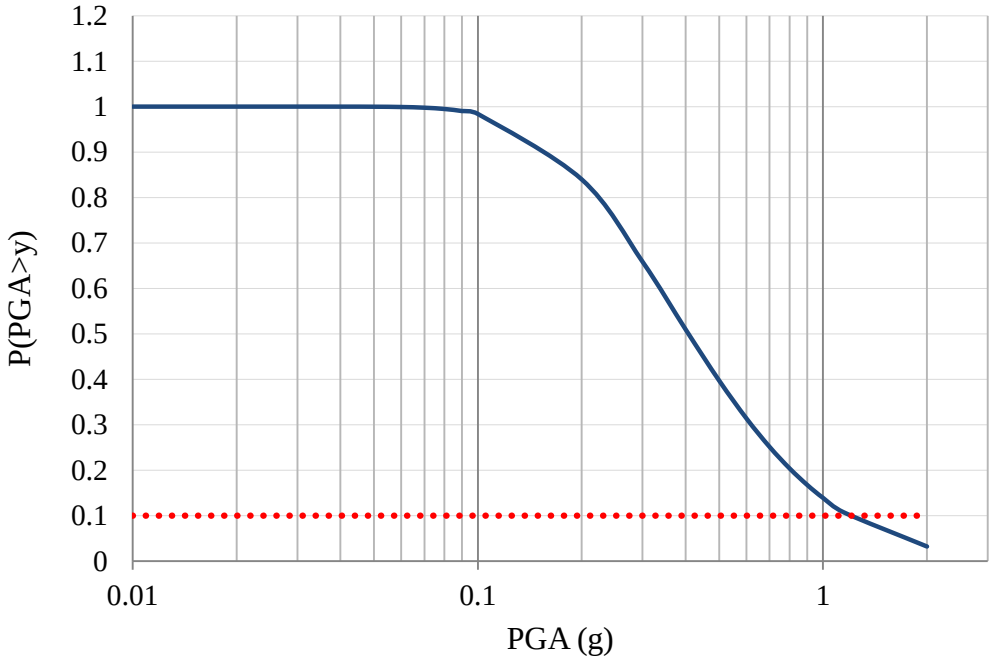

Picture 6 Cumulative hazard curve of 20 potential sources.10% exceedance probability level in 475-year return period is indicated in red dotted lines.

The critical acceleration (a_c) evaluated for the present slope model using Newmark's approach is 0.022g (equation 5). The obtained critical value (a_c) is substituted in the Jibson probabilistic model (equation 4), which provides the probability of landslide occurrence (Pr (DN(y_i)) in relation to ground shaking level (y_i). The conditional probability of slope failure (P_{ij}) in the next 50 years with respect to PGA is shown in Figure 7. The total probability of occurrence of the earthquake-induced landside in the next 50 years is 30%.

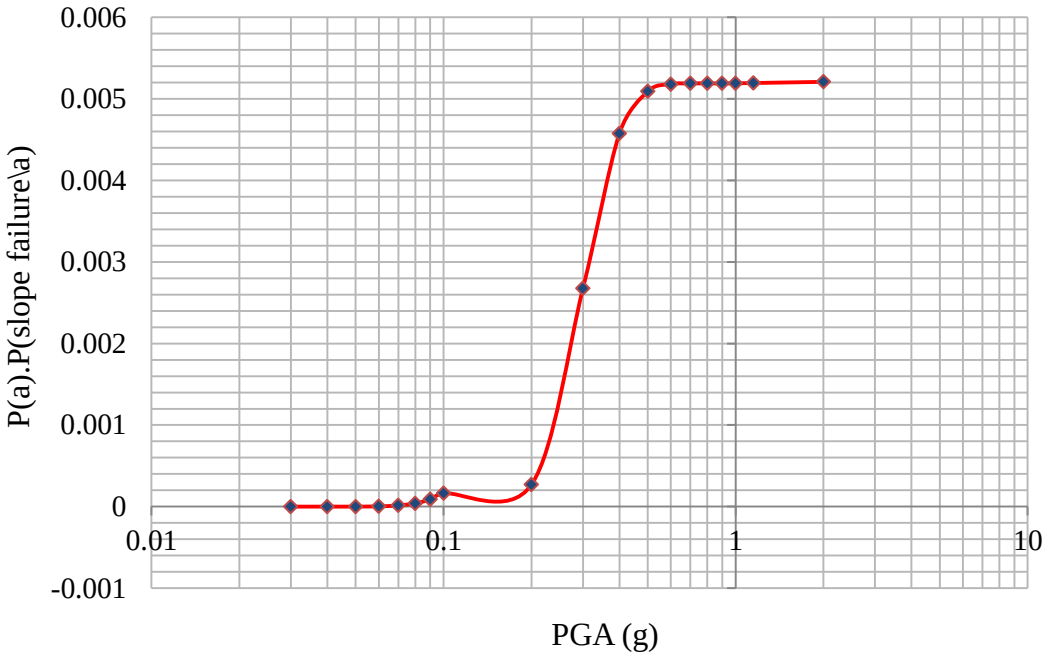

Picture 7 Total probability in next 50 years (cumulative distribution).

The (P_{ij}) obtained was multiplied by available ground scenario (a_i) for the slope model. For the considered slope model of critical acceleration (a_c), 0.022g of the PGA observed is approximately0.1–0.3g (Figure 8). The far variation in this PGA was observed for the 475-year probability.

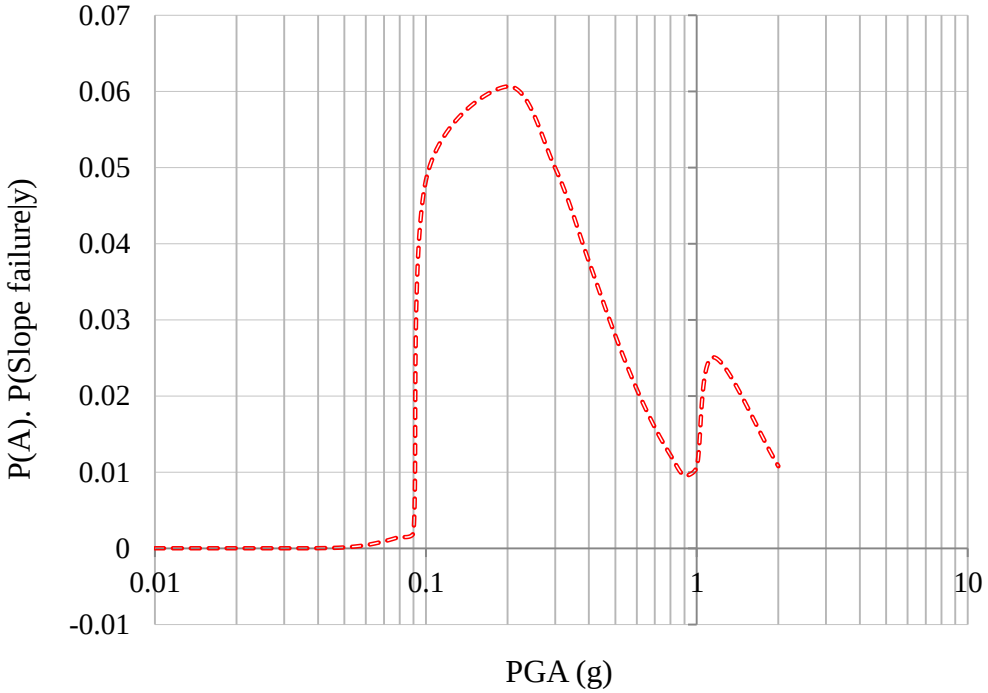

Picture 8 PDF of slope failure in next 50years

The PGA rates obtained from the 475-year shaking map intensity and fully probabilistic approach are 1.02g and 0.12g. Thus, the sliding displacements obtained from PSHA are much higher than those obtained by the fully probabilistic approach. The hazard deaggregation for estimating the most probable magnitude and distance from site to source has been performed in CRISIS software. The most probable earthquake scenario that would trigger the landslide in the next 50 years is M_w = 6.53 at a distance of R = 58km.

Conclusion

Ground shaking is an important factor in earthquake disasters. The appropriate ground motion is the key input in implementing risk mitigation measures and slope design. For the hazard assessment in the site, the improvised fully probabilistic technique is considered. The method is the multi-stage hazard approach that includes data selection, probabilistic seismic hazard analysis, geological investigations, and landslide probability calibration model.

The method is applied considering a Tindharia slope that is known asa seismically active slide from the past. A30% total probability of slope failure is observed in the next 50 years. The most probable seismic event obtained from fully probabilistic technique that would trigger the landslide in the next 50 years is PGA of 0.12g,M_w = 6.53, and R = 58km. The peak ground intensity predicted for the next 50 years from the probabilistic seismic hazard analysis is 1.02g. The corresponding Newmark's displacements predicted from the fully probabilistic approach are almost four times less than the sliding displacement obtained from the PGA of the 475-year return period.

The results depicted from the present study show that the significant difference in ground-shaking intensity is observed between the two methods. The landslide hazard is overestimated when considering the 475-year seismic hazard map obtained from the PSHA analysis. The fully probabilistic approach can handle all possible ground-motion scenarios and provide reasonable hazard management.

References:

1. Liao, H. W., and Lee, C. T. (2000). Landslides triggered by the Chi-Chi earthquake. *In Proceedings of the 21st Asian Conference on Remote Sensing*, Taipei. Vol.1, 2p.
2. Guzzetti, F., and Cardinali, M. (1990). Landslide inventory map of the Umbria region, Central Italy, *In: Proceedings ALPS 90 6th International Conference and Field Workshop on Landslides*, edited by: Cancelli, A., Milan, 273–284.
3. Lee, C.T., Huang, C.C., Lee, J.F., Pan, K.L., Lin, M.L., and Dong, J.J. (2008). Statistical approach to earthquake-induced landslide susceptibility. *Eng. Geol*. 100, 43–58.
4. Van Westen C.J., Castellanos, E., and Kuriakose, S.L. (2008). Spatial data for landslide susceptibility, hazard, and vulnerability assessment: an overview. *Eng. Geol*. 102 (3–4), 112-131.

5. Kanth, S. R., and Iyengar, R. N. (2007). Estimation of seismic spectral acceleration in peninsular India. *Journal of Earth System Science*. 116(3), 199-214.
6. Wang, T., Liu, J., Shi, J., and Wu, S. (2017). The influence of DEM resolution on seismic landslide hazard assessment based upon the Newmark displacement method: A case study in the loess area of Tianshui, China. *Environ. Earth Sci*. 76, 604.
7. Rathje, E.M., and Saygili, G. (2011). Estimating Fully Probabilistic Seismic Sliding Displacements of Slopes from a Pseudo probabilistic Approach. *J. Geotech. Geoenviron. Eng*. 137, 208–217.
8. Martino, S., Battaglia, S., Delgado, J., Esposito, C., Martini, G., and Missori, C. (2018). Probabilistic Approach to Provide Scenarios of Earthquake-Induced Slope Failures (PARSIFAL) Applied to the Alcoy Basin (South Spain). *Geosciences*. 8, 57p.
9. Alexey, K., Yuriy, G., and Andrey, S. (2020). Hazard-Consistent Earthquake Scenario Selection for Seismic Slope Stability Assessment. *MDPI. Sustainability.* 12, 4977p.
10. Del Gaudio, V., Wasowski, J., and Pierri, P. (2003). An Approach to Time-Probabilistic Evaluation of Seismically Induced Landslide Hazard. Bull. *Seismol. Soc. Am*. 93, 557–569.
11. Ketan Bajaj and Anbazhagan, P. (2019). Regional stochastic GMPE with available recorded data for active region –Application to the Himalayan region. *Soil dynamics and earthquake engineering*. 126, 105825.
12. Cornell, C.A. (1968). Engineering seismic risk analysis. *Bull. Seismol. Soc. Am*. 58, 1583–1606.
13. Newmark, N.M. (1965). Effects of earthquakes on dams and embankments. *Geotechnique.* 15, 139–159.
14. Romeo, R. (2000). Seismically induced landslide displacements: A predictive model. *Eng. Geol*. 58, 337–351.
15. Jibson, R.W., Harp, E.L., and Michael, J.A. (2000). A method for producing digital probabilistic seismic landslide hazard maps. *Eng. Geol*. 58, 271–289.
16. SEISAT. (2000). Seismotectonic Atlas of India, *Geological Survey of India*. New Delhi.
17. Scordilis, E. M. (2006). Empirical global relations converting Ms and Mb to moment magnitude. *Journal of seismology*. 10(2), 225-236.
18. Deniz, A., and Yucemen, M. S. (2010). Magnitude conversion problem for the Turkish earthquake data. *Natural hazards*. 55(2), 333-352.
19. Gardner, J. K., and Knopoff, L. (1974). Is the sequence of earthquakes in Southern California, with aftershocks removed, Poissonian?. *Bulletin of the Seismological Society of America*. 64(5), 1363-1367.
20. Stepp, J. C. (1973). Analysis of completeness of the earthquake sample in the Puget Sound area. NOAA Tech. Report ERL 267-ESL30, Boulder, Colorado.
21. Wiemer, S. (2001). A software package to analyze seismicity: ZMAP. *Seismol. Res. Lett*. 72(3) 373–382.
22. Kundu. (2019). Effect of rainfall and earthquake on landslides of Darjeeling Himalayas. Ph.D thesis. IIT Delhi.

23. Gutenberg, B., and Richter, C. F. (1944). Frequency of earthquakes in California; Bull. *Seismol. Soc. Am*. 34(4), 185–188.
24. Rydelek, P. A., and Sacks, I. S. (1989). Testing the completeness of earthquake catalogues and the hypothesis of self-similarity. *Nature*. 337(6204), 251–253.
25. Wiemer, S., and Wyss, M. (2000). Minimum magnitude of completeness in earthquake catalogs: examples from Alaska, the western US and Japan. *Bull Seism Soc A.* 90, 859–869.
26. Mitra, S., Bhattacharya, S.N., Nath, S.K. (2008), Crustal structure of the Western Bengal Basin from joint analysis of teleseismic receiver functions and Rayleigh-wave dispersion, Bull Seism Soc Am 98, 2715–2723.
27. S.K. Nath, K.K.S. Thingbaijam, J.C. Vyas, P. Sengupta, S.M.S.P. Dev. (2010), Macroseismic-driven site effects in the southern territory of West Bengal, India Seismological Research Letters, 81 (3), 480-482.